IMPACT: International Journal of Research in Applied, Natural and Social Sciences (IMPACT: IJRANSS)
ISSN (P): 2347-4580; ISSN (E): 2321-8851
Vol. 7, Issue 2, Feb 2019, 13-28

HETEROATOM RICH MESOPOROUS CARBON SUPPORTED GOLD NANOPARTICLES – AN EFFICIENT CATALYST FOR BENZYL ALCOHOL OXIDATION

Charitha Thambiliyagodage[1] & Martin G. Bakker[2]

[1]Research Scholar, Department of Chemistry, The University of Alabama, Tuscaloosa, Alabama, USA & School of Natural Sciences, Sri Lanka Institute of Information Technology, Sri Lanka

[2]Department of Chemistry, The University of Alabama, Tuscaloosa, Alabama, USA

Received: 22 Jan 2019 **Accepted:** 04 Feb 2019 **Published:** 11 Feb 2019

ABSTRACT

Hierarchically porous carbons containing oxygen (NC/O) and, oxygen and nitrogen (NC/O,N) were synthesized by nanocasting using furfuryl alcohol and furfuryl amine as the carbon precursors and hierarchically porous silica (SiO_2) monoliths as the template. Gold nanoparticles (Au NPs) supported on the nanocast carbons were synthesized by solution infiltration followed by reduction by heating in a hydrogen atmosphere. The materials were characterized by transmission electron microscope (TEM), scanning electron microscope (SEM), X-ray diffraction (XRD), X-ray photoelectron spectroscopy (XPS), Raman spectroscopy and N_2 adsorption for textural parameters determination. The mesoporous and macroporous structures of the SiO_2 template were well replicated in the nanocast carbons giving high surface area and mesopore volume. Au NPs were well dispersed on the carbon support and were in zero oxidation state. Amorphous carbon was present in all samples and a new type of disorder could be seen in NC/O,N consistent with the presence of nitrogen. Catalytic oxidation of benzyl alcohol by hydrogen peroxide showed that Au NPs on both NC/O and NC/O,N were catalytically active, with the NC/O,N supported Au NPs being more active and showing less decrease in activity with reuse.

KEYWORDS: *Heterogeneous, Nitrogen, Porous, Au NPs, Benzyl alcohol, Catalysis*

INTRODUCTION

The oxidation of alcohols is an interesting organic transformation that has been extensively studied using catalysts[1-6]. The selectivity of formation of a desired product depends strongly on the properties of the catalyst. Production of the corresponding acid from the alcohol after complete oxidation[7,8], the aldehyde by partial oxidation[9-12] or production of more than one product[6,13] has been reported in many studies. Nanoparticles (NPs) are attractive catalysts due to their high surface to volume ratio[14] but using NPs in homogeneous catalysis possess distinct disadvantages. Principally, the catalyst is hard to remove from the reaction mixture limiting the potential industrial use[15]. Product purification is therefore more difficult. Generally, in order to remove NPs they need to be aggregated and precipitated[16], which limits their reuse as catalysts.This is a major limitation for precious metal NPs and NPs that are expensive to synthesize[17]. NPs tend to aggregate to minimize the surface area when they are not covered by a ligand layer, reducing the catalytic activity. Even NPs passivated by ligands can aggregate in the reaction mixture due to changes in the chemical environment. In order to prevent such aggregation NPs are protected with capping agents such as

polymers[18] and dendrimers[19] that can assist in producing ultra small NPs. The drawbacks of NPs for homogeneous catalysis could be eliminated by stabilizing NPs onto a solid support as the solid catalysts could be easily removed from the reaction mixture[15,17]. Au NPs stabilized on solid supports have attracted interest for many chemical reactions like hydrogenation [20,21], oxidation[3,9] and coupling reactions[21]. Au NPs incorporated onto carbon supports including activated carbon, graphitic carbon and reduced graphene oxide have been investigated for catalytic activity in benzyl alcohol oxidation[22]. It has been reported that incorporation of two kinds of metal NPs like Au and Pd on activated carbon[13,23], carbon nanofibers[24], and mesoporous carbon[25] increases the catalytic activity. Furthermore, bimetallic NPs like Au and Pd on mesoporous carbon has shown high selectivity for conversion of benzyl alcohol to benzaldehyde[25]. In addition to carbon other supports including mesoporous SiO_2[26], ceria[27], and alumina[28] have also used as supports for Au NPs and bimetallic Au and Pd NPs. Carbon is particularly suitable as a support because carbon materials show high resistance to acids and bases, and the surface chemical structure and porosity can be well controlled[29]. In this work mesoporous carbons incorporating oxygen, and oxygen and nitrogen have been synthesized by using furfuryl alcohol (FA) and furfuryl amine as carbon precursors for nanocasting into mesoporous silica monoliths. $HAuCl_4$ was introduced into these mesoporous carbons by the incipient wetness method followed by reduction to form Au NPs. The catalytic activities of the resulting materials have been investigated for the benzyl alcohol oxidation reaction. The stability of Au NPs on oxygen and oxygen and nitrogen rich carbon has been evaluated.

MATERIALS AND METHODS

Materials

Polyethylene glycol PEG 35,000, nitric acid 70%, potassium hydroxide, benzyl alcohol, potassium carbonate, ethanol (95%), acetone and ethyl acetate were obtained from VWR. Aqueous ammonium hydroxide (NH_4OH, 29%) and hydrogen peroxide (30%) were purchased from Fisher Scientific. Furfuryl alcohol (FA) 98% and Furfuryl amine were purchased from Acros Organics. Tetraethyl orthosilicate (TEOS) 98% and anhydrous oxalic acid (OA) 98% were purchased from Alfa Aesar. Octadecyltrimethylammonium bromide (C_{18}TAB) was obtained from Genescript. $HAuCl_4.3H_2O$ 49% was purchased from Sigma-Aldrich. All chemicals were used as received without further purification.

Catalyst Synthesis

Synthesis of SiO_2 Monoliths

Synthesis of SiO_2 monoliths was carried out according to a literature procedure[32]. Briefly, PEG 35000 (2.2 g) was added to deionized water and was stirred until it completely dissolved. Then 6.5 ml of 30% HNO_3 was added to the stirring mixture. After that 32 ml of TEOS was added and stirred until a homogeneous mixture was obtained. C_{18}TAB (5.5 g) was then added and the mixture was stirred until all surfactant was dissolved. The resulted sol was degassed for a few minutes under low vacuum. They were poured into well plates and were incubated at 40 °C for 72 h. The gels were removed from the well plates and immersed in 1 M NH_4OH at 90 °C for 12 h. Then the monoliths were washed with 0.1 M HNO_3 and then washed with deionized water several times until the solution pH was within 1 unit of pH=7. The monoliths were then washed with acetone to remove residual water and dried at 40 °C for 72 h. The monoliths were calcined at 550 °C for 5 h at a heating rate of 1 °Cmin^{-1}.

Synthesis of NC/O

Preparation of NC/O was performed according to a modified version of a published procedure [49,50]. The SiO_2 monoliths, which are the templates for formation of the mesoporous carbon monoliths, were degassed for several hours prior to use. FA was diluted with ethanol in a 5:1 volume ratio, and OA was dissolved in the mixture at a molar ratio of FA: OA of 200:1. The SiO_2 monoliths were infiltrated in FA mixture for 12 h. The monoliths were then heated at 80 °C for 24 h to polymerize the FA. The infiltration and polymerization were repeated. The monoliths were heated to 800 °C under a flowing nitrogen atmosphere in 4 h and were held at that temperature for 2 h. After cooling, the monoliths were etched in 3 M KOH at 75 °C for 24 h in order to remove the SiO_2 template. They were then washed with deionized water several times and dried at room temperature.

Synthesis of NC/O,N

Synthesis of NC/O,N was carried out according to a modified version of an existing procedure[30]. The SiO_2 monoliths were degassed for several hours prior to use. They were infiltrated in furfuryl amine solution for 12 h. Then they were heated at 100 °C for 24 h and then at 160 °C for another 24 h in order to enhance the cross linking of the furfuryl amine. The infiltration and heating were repeated three times to provide sufficient robustness for the monolith to survive pyrolysis and etching. These were carried out as described above for NC/O.

Synthesis of Au NPs Supported NC

$HAuCl_4$ was introduced to mesoporous carbon by a solution infiltration method. Powdered NC was addedto $HAuCl_4$ (1 mg/ml) aqueous solution in which the Au concentration is prepared to be 1 wt% relative to the carbon weight. The suspension was stirred for 24 h at room temperature and then heated at 80 °C while stirring until the solution evaporated. Then the powder was washed three times with deionized water until no Cl^- ions were detected in washings. The powder was then dried at 70 °C for 24 h. To reduce the gold ions to metallic gold the powder was heated to 250 °C in 4 h and held at that temperature for 2 h in 5% H_2/N_2 flow.

Characterization

XRD patterns were collected by Bruker D2 phaser equipped with a Cu Kα source (Wavelength, 1.54 Å) Lynx-Eye 1D strip detector, and an anti-scatter blade fixed at 3 mm. The interlayer spacing, d was calculated from the Bragg equation, $d= \lambda/2\sin\theta$, in which λ is the wavelength of the Cu Kα x-ray source, θ is the Bragg angle and d is the interlayer spacing. Crystallite size (L_C) was calculated by the Debye-Scherrer equation, $L_C = K\lambda/B\cos\theta$, in which L_C is the crystallite size, K is the shape factor (0.9), and B is the full width at half maximum of the peak in radians. The acquisition time for all samples was 1 h. TEM images were obtained on a FET Tecnai F20, equipped with a cold field emission gun and a super twin objective lens with an accelerating voltage of 200 kV. Samples were prepared on holey carbon supported by a Cu grid. The morphology was imaged by bright field image.

Raman spectra were acquired by using a 10× objective lens and 532 nm laser wavelength as the excitation source. The laser power at the sample was kept around 0.5 mW to avoid heating effects. The spectra were deconvoluted with Lorentizian curves by using the peakfit software. A base line subtraction was performed before fitting the data. The region with frequencies ranging from 1200 to 1800 cm^{-1} (the D- and G-bands) was fitted with three bands. XPS were acquired on a Kratos Axis 165 XPS system that is operated with a dual Mg/Al anode and a monochromatic x-ray source at 1486.6

eV,corresponding to the Al Kα line. Photoelectrons were collected with a takeoff angle of 90° relative to the sample surface. Survey and high resolution spectra were acquired in order to determine the chemical states of C, O, N and Au. The survey spectra were taken at a pass energy of 160 eV, with a step size of 0.1 eV, using a single scan. The dwell time was 500 ms for the survey spectra and 1000 ms for the high resolution spectra. The peak deconvolution of all the high resolution spectra was performed using a Gaussian line shape.

SEM images were collected using a JEOL 7000 FE-SEM operated at 30 kV, with diode based back scatter detector and an Oxford EDS detector for elemental analysis. N_2 adsorption measurements were taken on a Quantachrome Nova 2200e pore size analyzer at -197 °C with He mode to determine the surface area and void volumes of the monoliths. The interpretation of the isotherms was carried out with Quantachrome Nova Win software version 11.03, using a multipoint BET method[51] to determine the surface areas and the BJH method[52] was applied to the adsorption branch to determine the pore size distribution. The volume of micropores was determined by the t-plot method. Product analysis was carried out on an HP 6890N gas chromatograph using a DB-1701 30 m × 320 µm × 1.0 µm column. A Waters Micromass Quattro micro mass spectrometer was used as detector.

Catalytic Tests

The oxidation of benzyl alcohol was carried outby using a batchreaction vessel with a refluxing condenser. Typically, the powdered catalyst (20 mg) was added into an appropriate volume of deionized water in a 50 ml round bottom flask. Then 0.4 mmol of K_2CO_3 (0.053g) was added while stirring followed by 0.2 mmol of benzyl alcohol. The reaction mixture was heated to 95 °C while refluxing and then 1 mmol of H_2O_2 (30%) was quickly added and the reaction mixture was stirred for 24 h. The contents of the flask were cooled to room temperature and transferred into a centrifuge tube. The flask was washed with 1 ml of ethyl acetate and that was also transferred into the centrifuge tube. Then the reaction mixture was centrifuged at 10,000 rpm for 1 h. The supernatant was collected and was centrifuged again using the same conditions and then that supernatant was filtered through a 0.2 µm filter. The pH of the filtrate was adjusted to 2 and then the reactants and products were extracted with ethyl acetate using 1 ml of ethyl acetate, repeated three times to ensure complete collection. The extracts were collected and a trace of water was removed using $MgSO_4$. The internal standard method was used for quantification, where the internal standard, toluene, was added to the extracted reactant and product mixture. Then reactants and products were analyzed by GC-MS.

Reusability study of the catalyst: the used catalyst was washed with deionized water twice, and separated by centrifugation at 10,000 rpm for 10 minutes and then used for the catalytic reaction as described above.

RESULTS AND DISCUSSIONS

Materials Characterization

Silica monoliths, cylindrical in shape and of about 7 mm in length and 5 mm of diameter, were used as templates for nanocasting carbon. Carbon monoliths made using FA will be referred to as NC/O as these monoliths have surface oxygen functionality after they are etched.Carbon monoliths made using furfuryl amine have added nitrogen and so will be referred to as NC/O, N. As described in the experimental section, NC/O monoliths showed shrinkage compared to the SiO_2 monoliths. When formed in the nanocasting process, NC/O,N appeared to be monoliths, but broke into pieces during polymerization of the furfuryl amine and during etching to remove the SiO_2. The SEM image in Figure **1a** shows the macropore structure of an SiO_2 monolith. SEM images in Figure **1b** and **c** show that the carbon produced by nanocasting

(NC/O and NC/O,N respectively) both show similar macropore structure to the SiO_2 monoliths. However, the macropore structure broke somewhat during grinding as shown in Figure **1d** and **e** for Au NPs supported on NC/O (NC/O/Au) and Au NPs supported on NC/O,N (NC/O,N/Au) respectively.

As noted in the experimental section (below) significantly more infiltrations with furfyl amine were required than produced monoliths from FA. This is likely a reflection of the underlying chemistry. The temperatures used for the polymerization of furfuryl amine were 100 °C and 160 °C where the latter temperature is greater than the boiling temperature of furfuryl amine which is 145 °C. The higher temperature. This leads to a trade-off: the higher temperature likely increases the rate of polymerization of furfuryl amine but at the price of faster evaporation. This evaporation will have led to the larger number of infiltration cycles required to form a replica (four for furfuryl amine compared with two for FA). It is also possible the extensive evaporation and the large amounts of gaseous furfuryl amine may also be the cause of the extensive fracturing of the template observed. It is difficult to tell if this was also an issue for other examples of furfuryl amine nanocasting reported[30] as this was nanocasting into SiO_2 powders for which any fracturing produced would not be noticed. However, for that report[30] only two nanocasting cycles were reported as being necessary. This may reflect the incorporation of $FeCl_3$: as we have previously reported for FA[31] nanocasting, transition metal salts such as $FeCl_3$ added during the nanocasting process are sufficient acidic to act as acid catalyst.

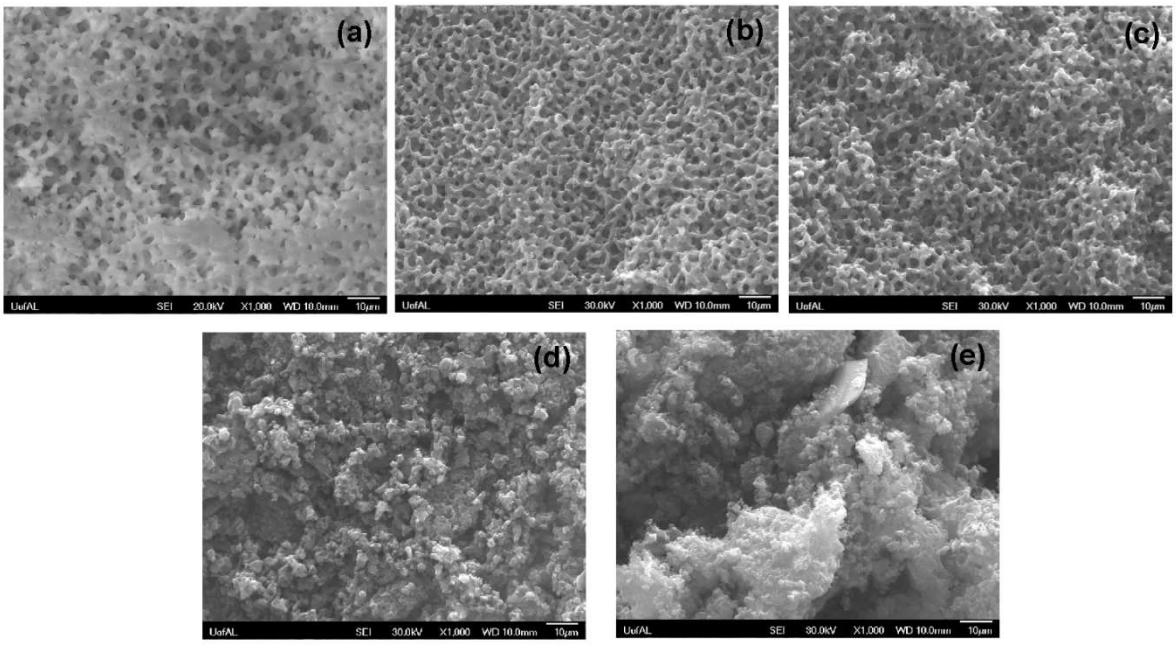

Figure 1: The SEM images of (a) SiO_2(b) NC/O (c) NC/O,N(d) NC/O/Au (e) NC/O,N/Au

The nitrogen isotherms and pore size distribution plots of template and replicated materials are given in Figure **2a** and **2b,** respectively, and the values of the textural parameters are given in Table 1. The nitrogen sorption isotherm of SiO_2 shows two regions of N_2 uptake. The first N_2 uptake region around P/Po = 0.4 is due to the surfactant mesopores and the second uptake region round P/Po = 0.9 is due to the textural mesopores[32]. In isotherms of both NC/O and NC/O,N the uptake around relative pressure of 0.9 is almost absent indicating that the textural mesopores in the SiO_2 templates are completely filled with carbon. But the uptake around relative pressure of 0.4 indicates the presence of surfactant mesopores in both types of carbon. The BJH pore size distribution shows a narrow peak at 3.4 nm in SiO_2 which is consistent with the

octadecyl trimethylammonium bromide (C_{18}TAB) used as a porogen to make SiO_2. The maxiuma in the pore size distributions for NC/O and NC/O,N are 3.2 nm and 4.4 nm, respectively, but the pore size distributions are much broader than in the SiO_2templates. This is consistent with earlier work[33,34] andclearly shows that the mesopore structure is replicated in both NC/O and NC/O,N. The broad pore size distributions in the nanocast materials (NC/O and NC/O,N) result from the variable mesopore wall thickness in the SiO_2 monolith, because the surfactant mesopores are randomly organized rather than an ordered array. Since both types of carbon produced via nanocasting are negative replicas of the mesopores they show a broader pore size distribution. The isotherms and pore size distributions of NC/O/Au and NC/O,N/Au show similar behavior to NC/O and NC/O,N, with minor differences in surface areas and pore volumes which are not believed to be significant.

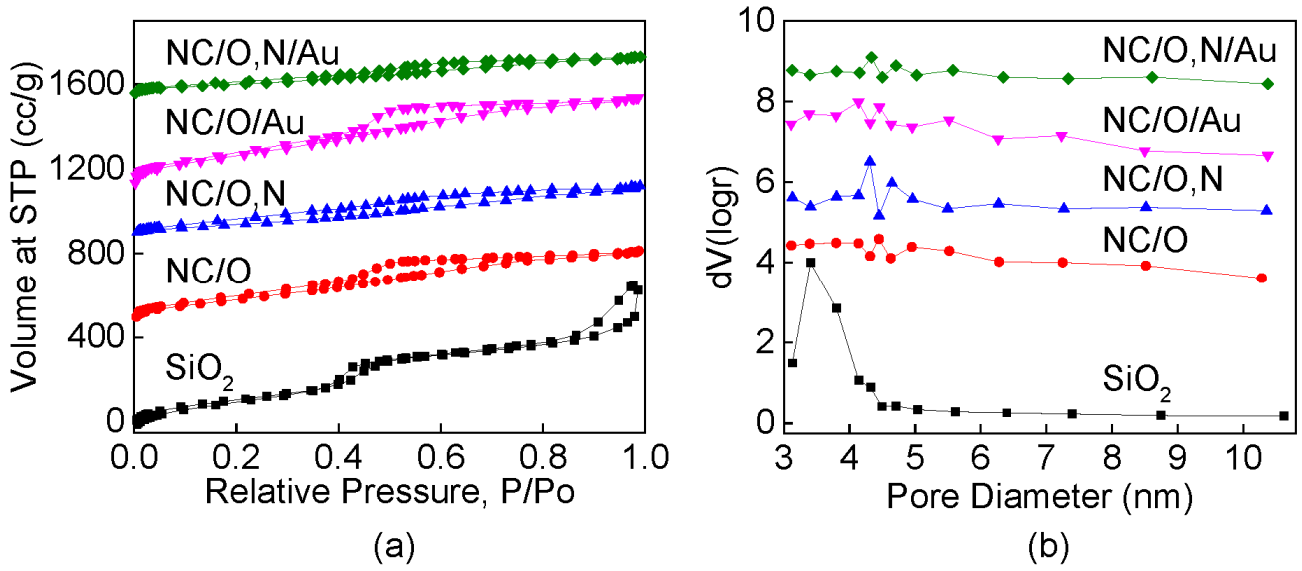

Figure 2: (a) N_2 Sorption Isotherms and (b) BJH Pore Size Distributions of Template and Replicated Materials

Table 1: Textural Parameters of Template and Replicated Materials

Sample	BET Surface Area (m^2/g)	Total Pore Volume (cc/g)	Mesopore Volume (cc/g)	Micropore Volume (cc/g)	BJH Pore Diameter (nm)
SiO_2	673	0.62	0.62	0.00	3.4
NC/O	650	0.48	0.48	0.00	3.2
NC/O,N	222	0.19	0.19	0.00	4.4
NC/O/Au	781	0.58	0.58	0.00	4.2
NC/O,N/Au	203	0.18	0.18	0.00	4.4

TEM images of NC/O/Au and NC/O,N/Au are given in Figure **3a** and **b,** respectively. The corresponding gold nanoparticle size distributions are given in Figure **3c** and **d,** respectively. The Au NPs are well distributed on the carbon matrix at this length scale, but have a relatively wide range of particle sizes as can be seen in the TEM images and particle distribution histograms. Qualitatively the Au NPs appear to be better dispersed for the NC/O,N/Au sample than in the NC/O/Au sample. The average particle sizes are 39 nm and 25 nm respectively, in NC/O/Au and NC/O,N/Au. In both samples nanoparticleswere observed that appear to be formed by partial merging of two or more spherical particles. Two mechanisms can be envisaged that would give this result: one in which reduction in a $AuCl_3$ nanoparticle starts at multiple locations each of which grows to give a spherical particle leading to the observed conjoined spheres.Alternately, Au NPs

formed during the reduction process could move across the carbon surface and start to sinter, but not be completely mergedduringthe reduction process.

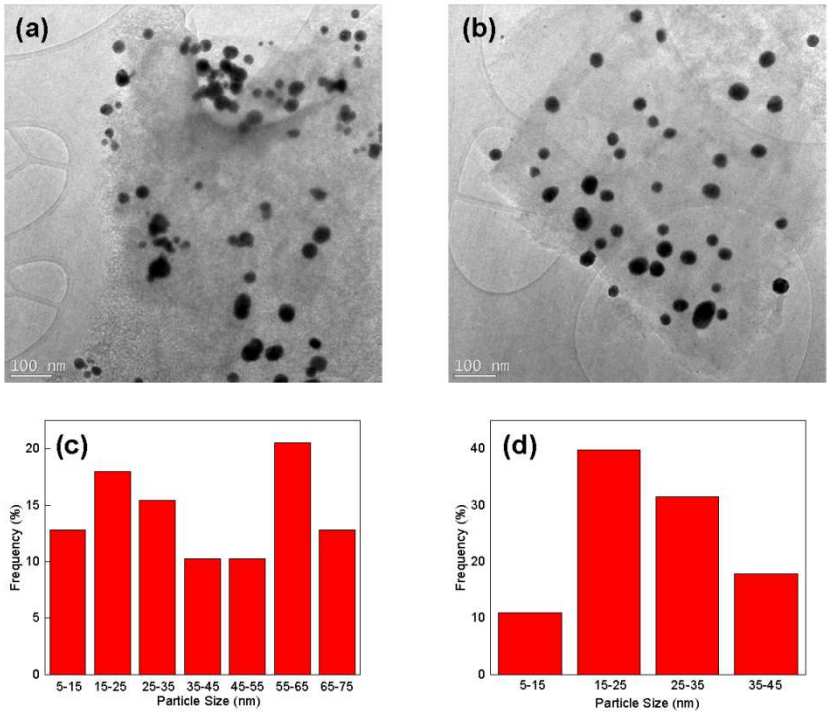

Figure 3: TEM Images of (a) NC/O/Au (b) NC/O,N/Au Particle Size Distributions of (c) NC/O/Au (d) NC/O,N/Au

The SEM images of NC/O/Au and NC/O,N/Au taken with a backscatter detector (COMPO) are given in Figure **4a** and **b,** respectively. Those images show that the NPs are distributed on the macropores and show that in addition to the dispersed NPs, aggregated NPs are also present. These images also show that NPs are heterogeneously distributed on the macropores. The metal loading relative to carbon was 1 wt%, which is relatively low. The method used to introduce metal precursor was solution infiltration where the precursor solution was stirred with the carbon powder while heating until all the solution evaporated. The size and distribution of the $AuCl_3$ nanoparticles will depend upon the concentration and distribution of any surface nucleation sites compared to the volume of solution remaining when the saturation concentration of the $AuCl_3$ is reached. A high number of surface sites would be expected to yield smaller nanoparticles, whereas a lower number would produce larger $AuCl_3$ particles and so larger Au NPs.The particle size distribution would therefore depend upon the number, distribution and nature of oxygen and nitrogen surface functional groups. The atomic percentage of oxygen relative to carbon determined by XPS (below) is 3.53 % and 3.34% in NC/O/Au and NC/O,N/Au respectively, and that of nitrogen of NC/O,N/Au is 5.07%. That the average particle size observed by TEM is smaller for NC/O,N/Au than for NC/O/Au is consistent with the nitrogen acting as a nucleation site for $AuCl_3$ binding and reduction.

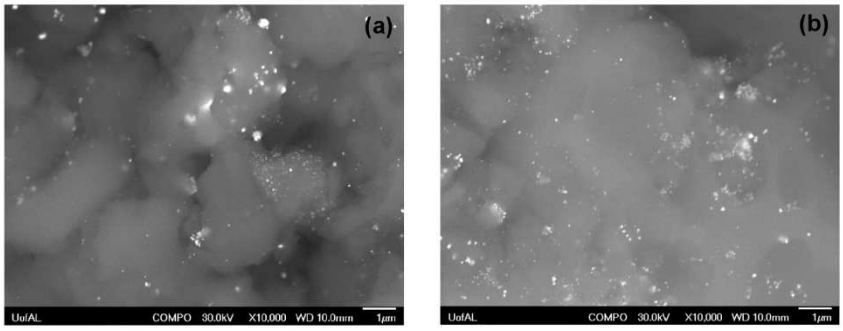

Figure 4: SEM Images of (a) NC/O/Au (b) NC/O,N/Au Taken using the Back Scatter Detector

The wide angle XRD patterns are given in Figure **5**. The XRD patterns of NC/O and NC/O,N show a broad peak around 2θ, 23.5° indicating the presence of amorphous carbon. In addition to that there is another small broad peak around 43.7° which is due to scattering from carbon (10) and (100) planes. The XRD patterns of NC/O/Au and NC/O,N/Au show peaks at 38.4°, 44.6°, 64.8°, 77.6° and 81.8° which could be assigned to diffractions of (111), (200), (220), (311), and (222) of fcc metallic Au. Debye-Scherrer analysis was performed on (111) diffraction peak of NC/O/Au and NC/O,N/Au to determine the crystallite size of the Au crystals. The crystallite size calculated for NC/O/Au is 23.7 nm and for NC/O,N/Au it is 20.1 nm. The d-spacings were also calculated by using the (111) diffraction peak and they are 0.2345 nm and 0.2341 nm in NC/O/Au and NC/O,N/Au respectively. The crystallite sizes found by XRD although smaller than those found by are consistent with the TEM images, as a number of the particles were formed from multiple crystallites.

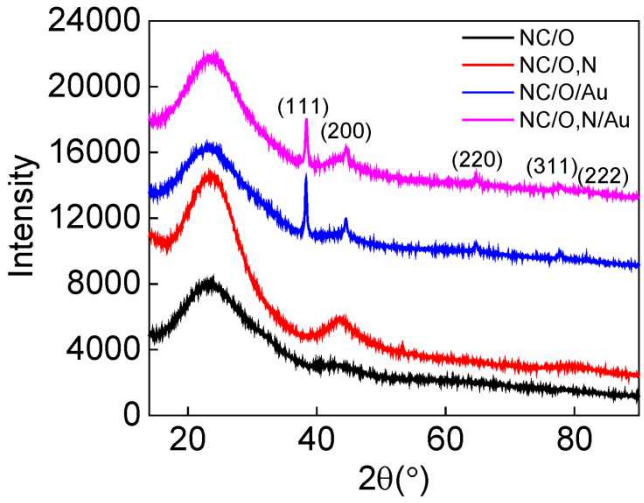

Figure 5: The Wide Angle XRD Patterns

Carbon materials are characterized by Raman spectroscopy to determine the vibrational modes of the material, which can be interpreted to give insight into the atomic level structure of the carbon. The Raman spectra of NC/O, NC/O,N, NC/O/Au, and NC/O,N/Au are shown in Figure **6 a, b, c,** and **d,** respectively. The G band appeared around 1600 cm^{-1} corresponding to the zone center phonons of E_{2g} symmetry and the D band appeared around 1350 cm^{-1} corresponds to the *K*- point phonons of A_{1g}symmetry [35,36]. The G band is due to the bond stretching of sp^2 atoms in both rings and chains and the D band is due to the breathing modes of sp^2 atoms in six membered rings[37]. The third peak in between the D and G band is added to get a better fit, and is believed to be from a combination of sp^2 and sp^3 carbons that have not crystallized [35,38-40]. The D band appeared at about 1347 cm^{-1} in NC/O and in NC/O/Au but in NC/O,N and NC/O,N/Au

it appeared at about 1359 cm^{-1}. The shift of the D band in nitrogen functionalized carbon indicates a new type of disorder compared to the oxygen functionalized carbon[41]. The G band was not shifted. The intensity ratio of the D and G bands is the same in all samples indicating that there is no change in crystallinity in carbon by incorporation of nitrogen.

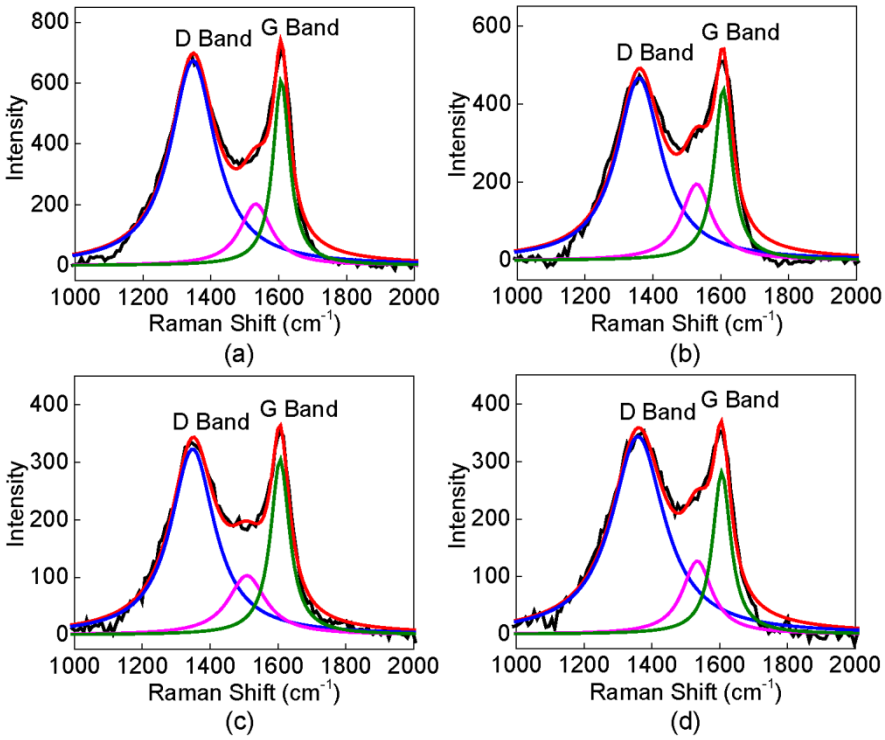

Figure 6: Raman Spectra of (a) NC/O (b) NC/O,N (c) NC/O/Au (d) NC/O,N/Au

The high resolution XPS spectra (Figure **7**) were acquired in order to determine the chemical states of the elements of the catalysts. The high resolution spectra of the C 1s for NC/O/Au (Figure **7a**) shows sp^2 hybridized C-C at 284.4 eV and that in NC/O,N/Au (Figure **7b**) is observed at 286.3 eV. The C-O feature appears at 285.7 eV in the high resolution spectrum of C 1s of NC/O/Au. The various forms of C-N also appear in the region of 285-287 eV[42]. So in the high resolution spectrum of C 1s of NC/O,N/Au the peak at 285.6 eV is assigned to C-O and C-N features. The peak at 287.5 eV in C 1s of NC/O/Au and NC/O,N/Au corresponds to the C=O bond[43]. The higher binding energy peak at about 290 eV for both NC/O/Au and NC/O,N/Au can be assigned to a shake-up peak. The high resolution spectra of O 1s of NC/O/Au and NC/O,N/Au are given in Figure **7c** and **d,** respectively. The peaks appearing around 531 eV correspond to the C=O bond, the peaks around 532 eV are assigned to the C-O bond[43] and the peaks around 533.8 eV can be assigned to O-H bonds[42]. The high resolution spectrum of N 1s of NC/O,N/Au is shown in Figure **7e**. The peak at 399.9 eV is assigned to pyrrolic N[44] where N is bound to two C atoms and the peak at 403.6 eV corresponds to oxidized N. It can be considered that furfuryl amine forms pyrrolic N when N is present in a five member ring bound to two C atoms during pyrolysis and it does not form any graphitic N which should appear at around 401 eV[45]. The oxidized N could be due to the KOH used for etching. The high resolution spectra of Au 4f of NC/O/Au and NC/O,N/Au are given in Figure **7f** and **g,** respectively. The Au $4f_{7/2}$peak in NC/O/Au appeared at 84.4 eV and that of NC/O,N/Au at 83.9 eV indicating that the oxidation state of the surface of Au NPs is zero. That the binding energy of Au $4f_{7/2}$for NC/O/Au is slightly higher is attributed to slight charging of the sample. That the gold surface remains unoxidized is consistent with the relative

inertness of Au. The elemental composition as atomic percentage relative to carbon is given in table 2. That the atomic percentage of oxygen in NC/O/Au (3.53%) is higher than in NC/O,N/Au (3.35%) is not surprising, as thereare two oxygen atoms in furfuryl alcohol and one oxygen atom in furfuryl amine. That the difference is not in the ratio of 2:1 can be attributed to a number of factors, including differences in pyrolysis mechanisms, and potential contributions to the oxygen signal from the OH ions from the KOH used to etch SiO_2, and reactions with atmospheric oxygen and H_2O vapor. The atomic nitrogen percentage relative to carbon, 5%, indicates reasonably high nitrogen incorporation has been achieved by using furfuryl amine as the nitrogen precursor. That it is less than the approximately 23% nitrogen in the amine precursor indicates that nitrogen is preferentially lost during the carbonization procedure. The atomic percentages of Au are 0.09% and 0.14% in NC/O/Au and NC/O,N/Au respectively. They can be considered as similar within the error range as they are only a little above the detection threshold for XPS.

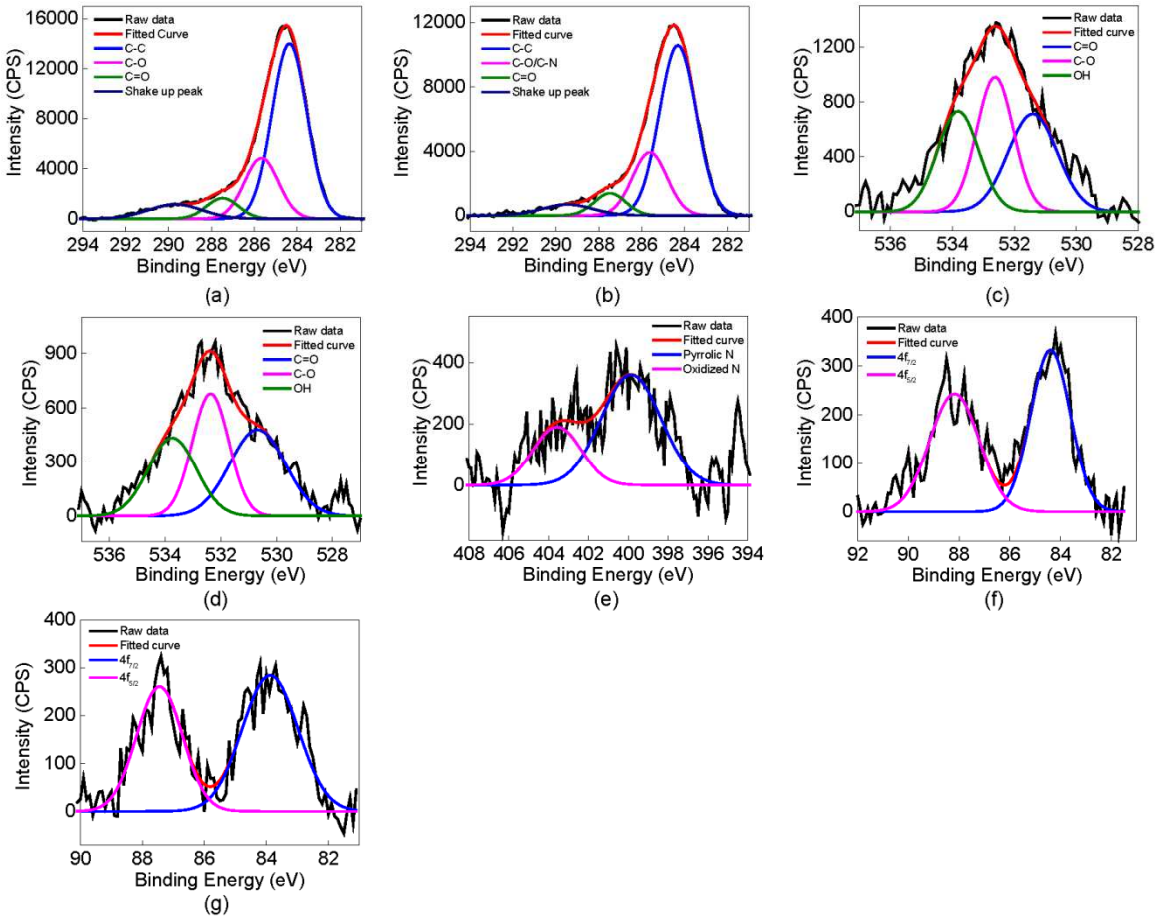

Figure 7: High Resolution XPS Spectra of, C 1s of (a) NC/O/Au (b) NC/O,N/Au, O 1s of (c) NC/O/Au (d) NC/O,N/Au, N 1s of (e) NC/O,N/Au, Au 4f of (f) NC/O/Au (g) NC/O,N/Au

Table 2: Atomic Percentages Relative to C based on XPS Quantification

Catalyst	Atomic Percentage Relative to C		
	O	N	Au
NC/O/Au	3.53	-	0.094
NC/O,N/Au	3.34	5.07	0.14

Catalytic Activity

The catalytic activity found is summarized in Figure 8 which shows the extent of conversion and the selectivity for formation of benzaldehyde and benzoic acid. Fresh NC/O/Au catalyst gave 81.5% conversion compared to 91.5% conversion by NC/O,N/Au. NC/O/Au had a high selectivity for benzoic acid (96.7%) compared to 3.3% of benzaldehyde. Fresh NC/O,N/Au showed somewhat higher activity (90%) but significantly lower selectivity for benzoic acid (61.4%) with a commensurate increase in benzaldehyde formation (38.6%). The turn over number (TON) and turn over frequency (TOF) found for NC/O/Au were 0.815 mol/g and 0.034 mol/g.h, and 0.915 mol/g and 0.038 mol/g.h for NC/O,N/Au. The higher conversion observed for NC/O,N/Au is not surprising, as the smaller nanoparticles in NC/O,N/Au would have a surface area approximately twice that of NC/O/Au. The difference in product selectivity is rather interesting: the primary product for both catalysts is benzoic acid, but the selectivity is higher for NC/O/Au, the less active catalyst, suggesting that there may be differences in the mechanism for the two catalysts.

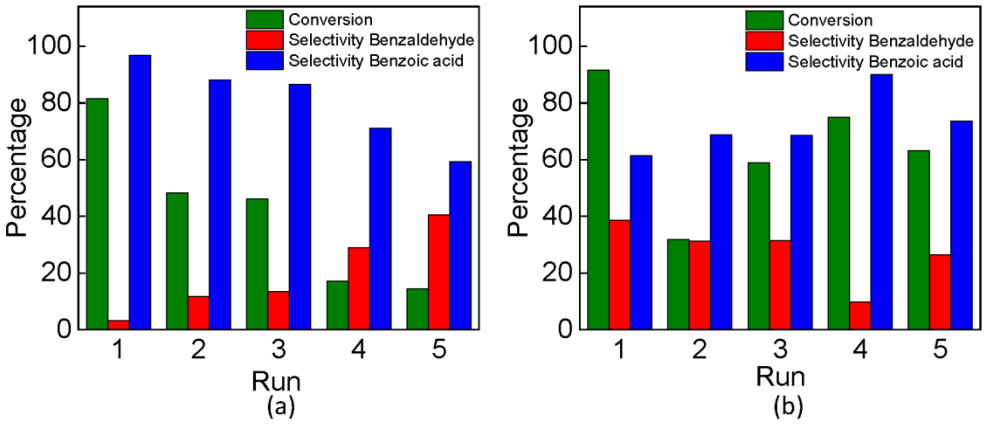

Figure 8: Reusability Study of (a) NC/O/Au (b) NC/O,N/Au

The recyclability results are also rather interesting. For the NC/O/Au the percentage conversion drops rapidly: from 81% in the first run to about 15% in the 5th experiment. This drop is matched by changes in the selectivity, with less benzoic acid and more benzaldehyde being formed.For NC/O,N/Au the scatter in the data is significantly larger and with no statistically significant change in overall conversion being seen. There does appear to be a trend in the selectivity which decreases for benzaldehyde and increases for benzoic acid, however the correlation coefficient is only R^2=.45 which gives a slope significant at the 68% confidence level but not at the 95% confidence level.

To determine the cause of the drop in activity of the NC/O/Au catalyst, SEM images were taken with a back scatter detector (COMPO) of NC/O/Au and NC/O,N/Au after five cycles of catalysis (shown in Figures **9a** and **b,** respectively). Since the images were not obtained from the same sample and positions as those in Figure 4 a direct comparison is not possible and it is not clear that there are major differences in the number, size and extent of agglomeration of the Au NPs as seen at the magnification used for the SEM. This would tend to rule out large loss of particles from the surface of the carbon. It is still possible that there were changes in the size distribution resulting in a lower gold surface area, but this can not be determined from the SEM images.

The differences in behavior of NC/O/Au compared to NC/O,N/Au for benzyl alcohol oxidation suggest that there are significant differences in activity. An XANES experiment found that the electronic properties of 3 nm and 9 nm diameter Au NPs incorporated into a mesoporous carbon were significantly different,[46] and the smaller particles were

observed to be significantly more active. However, in our experiment the two sets of supported Au NPs used are both relatively large and almost certainly above the limit at which quantum effects might be expected. Further, Jawale et al.[47] reported that the difference in reactivity of 3 and 20 nm Au NPs supported on carbon nanotubes could be completely explained by the differences in surface area.

It seems possible therefore that the presence of the nitrogen impacts the activity of the catalyst, in ways beyond impacting the average Au NP size. This is perhaps not surprising as nanoporous graphitic carbon nitride (g-C_3N_4) without any metals is reported to be an effective catalyst for oxidation of toluene to benzaldehyde by molecular oxygen[48].Interestingly, the presence of the g-C_3N_4 acts to suppress the homogenous auto-oxidation of the benzyl alcohol and benzaldehyde formed from toluene to give benzoic acid and other products. This is suggested to occur due to trapping of the superoxide radical anion ($\bullet O_2^-$).We have used hydrogen peroxide which is a more aggressive oxidant. At the basic pH used hydrogen peroxide is approximately 90% ionized and so trapping of HO_2^- on the surface could significantly impact the reaction pathway. Oxygen species could bind to or react with nitrogen to give active N=O that could act as an intermediate.

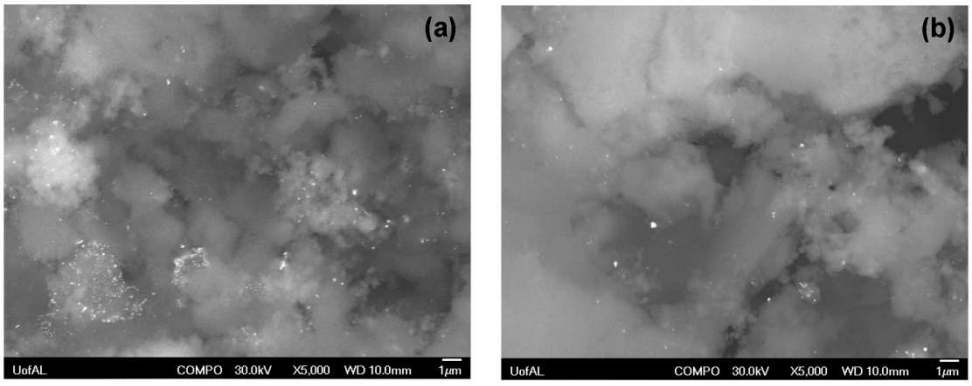

Figure 9: SEM Images of the used Catalysts after Five Cycles of (a) NC/O/Au (b) NC/O,N/Au Taken from the Back Scatter Detector

CONCLUSIONS

Oxygen, and oxygen and nitrogen rich hierarchically porous carbons were synthesized by nanocasting of furfuryl alcohol and furfuryl amine respectively into a mesoporous SiO_2 template. Unlike the oxygen only carbon, the nitrogen rich carbon could not be formed as a monolith. This was ascribed to the reduced precursor polymerization in the absence of added transition metal or other acid catalyst.With less polymerization, the furfuryl amine evaporated giving lower carbon yield and higher gas volumes which are suggested to be the cause of the observed fracturing of the silica template. $HAuCl_4$ was introduced by a solution infiltration method followed by reduction in 5% H_2/N_2 to produce AuNPs supported on the two carbons. The nitrogen rich carbon gave significantly smaller Au NPs. These catalysts were able to catalyze the oxidation of benzyl alcohol by H_2O_2. Nitrogen rich catalysts werefound to be more active than oxygen only catalysts, with a somewhat different product distribution. The oxygen only catalysts rapidly lost activity, whereas the nitrogen rich catalyst showed less reduction in activity with reuse.

ACKNOWLEDGMENTS

The Central Analytical Facility of the University of Alabama and the required cost match from the Bakker Gift Fund is acknowledged. The authors acknowledge Drs. Greg Szulczewski, Paulo T. Araujo, Kevin Shaughnessy, and Carolyn Cassady for valuable discussions. Authors thank Dr. J. Allred for use of his XRD instrument and David Matetich for collecting the XRD patterns. The authors also thank Steven Ulrich for acquiring Raman spectra.

Conflicts of Interest: The authors declare no conflict of interest.

REFERENCES

1. *He, Y.; Yang, P.; Fan, J.; Liu, Y.; Du, Y.; Feng, J.; Fan, F.; Li, D. (2015). Facile and surfactant-free synthesis of supported Pd nanoparticles on hydrotalcite for oxidation of benzyl alcohol. RSC. Adv.5, 74907-74915.*
2. *Hou, W.; Dehm, N.A.; Scott, R.W.J. Alcohol oxidations in aqueous solutions using Au, Pd, and bimetallic AuPd nanoparticle catalysts. (2008)Journal of Catalysis, 253, 22-27.*
3. *Kumar, A.; Kumar, V.P.; Srikanth, A.; Vishwanathan, V.; Chary, K.V.R. Vapor Phase Oxidation of Benzyl Alcohol over Nano Au/SBA-15 Catalysts: Effect of Preparation Methods. Catalysis Letters. 146, 35-46.*
4. *Ma, C.Y.; Dou, B.J.; Li, J.J.; Cheng, J.; Hu, Q.; Hao, Z.P.; Qiao, S.Z. (2009). Catalytic oxidation of benzyl alcohol on Au or Au–Pd nanoparticles confined in mesoporous silica. Applied Catalysis B: Environ. 92, 202-208.*
5. *Mallat, T.; Baiker, A. (1994) Oxidation of alcohols with molecular oxygen on platinum metal catalysts in aqueous solutions. Cataylysis Today, 19, 247-284.*
6. *Villa, A.; Janjic, N.; Spontoni, P.; Wang, D.; Su, D.S.; Prati, L. (2009). Au–Pd/AC as catalysts for alcohol oxidation: Effect of reaction parameters on catalytic activity and selectivity. Applied Catalysis A, 364, 221-228.*
7. *Anderson, R.; Griffin, K.; Johnston, P.; Alsters, P.L. (2003). Selective Oxidation of Alcohols to Carbonyl Compounds and Carboxylic Acids with Platinum Group Metal Catalysts. Advanced Synthesis Catalysis,345, 517-523.*
8. *Ji, H.; Mizugaki, T.; Ebitani, K.; Kaneda, K. (2002). Highly efficient oxidation of alcohols to carbonyl compounds in the presence of molecular oxygen using a novel heterogeneous ruthenium catalyst. Tetrahedron Letters, 43, 7179-7183.*
9. *Long, N.Q.; Quan, N.A. (2015). Highly selective oxidation of benzyl alcohol to benzaldehyde catalyzed by nano Au/y-Al2O3 under environment-friendly conditions. Reaction Kinetics, Mechanisms and Catalysis,114:, 147-155.*
10. *Zhan, B.-Z.; White, M.A.; Sham, T.-K.; Pincock, J.A.; Doucet, R.J.; Rao, K.V.R.; Robertson, K.N.; Cameron, T.S. (2003). Zeolite-Confined Nano-RuO2: A Green, Selective, and Efficient Catalyst for Aerobic Alcohol Oxidation. Journal of American Chemical Society, 125, 2195-2199.*
11. *Ji, H.-B.; Ebitani, K.; Mizugaki, T.; Kaneda, K. (2002). Environmentally friendly alcohol oxidation using heterogeneous catalyst in the presence of air at room temperature. Catalysis Communication,3, 511-517.*

12. *Mahyari, M.; Shaabani, A.; Behbahani, M.; Bagheri, A. (2014). Thiol-functionalized fructose-derived nanoporous carbon as a support for gold nanoparticles and its application for aerobic oxidation of alcohols in water. Applied Organometallic Chemistry, 28, 576-583.*

13. *Pritchard, J.; Kesavan, L.; Piccinini, M.; He, Q.; Tiruvalam, R.; Dimitratos, N.; Lopez-Sanchez, J.A.; Carley, A.F.; Edwards, J.K.; Kiely, C.J., et al.(2010). Direct Synthesis of Hydrogen Peroxide and Benzyl Alcohol Oxidation Using Au-Pd Catalysts Prepared by Sol Immobilization. Langmuir, 26, 16568-16577.*

14. *Chaturvedi, S.; Dave, P.N.; Shah, N.K. (2012). Applications of nano-catalyst in new era. Journal of Saudi Chemical Society,16, 307-325.*

15. *Gruber-Woelfler, H.; Radaschitz, P.F.; Feenstra, P.W.; Haas, W.; Khinast, J.G. (2012). Synthesis, catalytic activity, and leaching studies of a heterogeneous Pd-catalyst including an immobilized bis(oxazoline) ligand. Journal of Catalysis,286, 30-40.*

16. *Yuan, Y.; Yan, N.; Dyson, P.J. (2011). pH-Sensitive Gold Nanoparticle Catalysts for the Aerobic Oxidation of Alcohols. Inorganic Chemistry,50,, 11069–11074.*

17. *Cole-Hamilton, D.J. (2003). Homogeneous Catalysis—New Approaches to Catalyst Separation, Recovery, and Recycling. Science, 299, 1702-1706.*

18. *Tsunoyama, H.; Sakurai, H.; Ichikuni, N.; Negishi, Y.; Tsukuda, T. (2004). Colloidal Gold Nanoparticles as Catalyst for Carbon-Carbon Bond Formation: Application to Aerobic Homocoupling of Phenylboronic Acid in Water. Langmuir, 20, 11293-11296.*

19. *Garcia-Martinez, J.C.; Lezutekong, R.; Crooks, R.M. (2005). Dendrimer-Encapsulated Pd Nanoparticles as Aqueous, Room-Temperature Catalysts for the Stille Reaction. Journal of American Chemical Society, 127, 5097-5103.*

20. *Gu, H.; Xu, X.; Chen, A.-a.; Ao, P.; Yan, X. (2013). Separate deposition of gold and palladium nanoparticles on ordered mesoporous carbon and evaluation of their catalytic activity for cinnamaldehyde hydrogenation under atmospheric condition. Cataysis Communication, 41, 65-69.*

21. *Datta, K.K.R.; Reddy, B.V.S.; Ariga, K.; Vinu, A. (2010). Gold Nanoparticles Embedded in a Mesoporous Carbon Nitride Stabilizer for Highly Efficient Three-Component Coupling Reaction. Angewantde Chemie International Edition, 49, 5961-5965.*

22. *Yu, X.; Huo, Y.; Yang, J.; Chang, S.; Ma, Y.; Huang, W. (2013). Reduced graphene oxide supported Au nanoparticles as an efficient catalyst for aerobic oxidation of benzyl alcohol. Applied Surface Science, 280, 450-455.*

23. *Di Wang; Alberto Villa; Paolo Spontoni; Dang Sheng Su; Prati, L. (2010). In Situ Formation of Au–Pd Bimetallic Active Sites Promoting the Physically Mixed Monometallic Catalysts in the Liquid-Phase Oxidation of Alcohols. Chemistry-A Europian Journal. 16, 10007-10013.*

24. *Villa, A.; Wang, D.; Spontoni, P.; Arrigo, R.; Su, D.; Prati, L. (2010). Nitrogen functionalized carbon nanostructures supported Pd and Au–Pd NPs as catalyst for alcohols oxidation. Catalysis Today, 157, 89-93.*

25. *Hao, Y.; Hao, G.-P.; Guo, D.-C.; Guo, C.-Z.; Li, W.-C.; Li, M.-R.; Lu, A.-H. (2012). Bimetallic Au–Pd Nanoparticles Confined in Tubular Mesoporous Carbon as Highly Selective and Reusable Benzyl Alcohol Oxidation Catalysts. ChemCatChem, 4, 1595-1602.*

26. *Wang, L.; Meng, X.; Wang, B.; Chi, W.; Xiao, F.-S. (2010). Pyrrolidone-modified SBA-15 supported Au nanoparticles with superior catalytic properties in aerobic oxidation of alcohols. Chemical Communications, 46, 5003-5005.*

27. *Zhang, H.; Xie, Y.; Sun, Z.; Tao, R.; Huang, C.; Zhao, Y.; Liu, Z. (2010). In-Situ Loading Ultrafine AuPd Particles on Ceria: Highly Active Catalyst for Solvent-Free Selective Oxidation of Benzyl Alcohol. Langmui, 27, 1152-1157.*

28. *Pawelec, B.; Venezia, A.M.; La Parola, V.; Cano-Serrano, E.; Campos-Martin, J.M.; Fierro, J.L.G. (2005). AuPd alloy formation in Au-Pd/Al2O3 catalysts and its role on aromatics hydrogenation. Applied Surface Science, 242, 380-391.*

29. *Rodriguez-Reinoso, F.(1998). The Role of Carbon Materials in Heterogeneous Catalysis. Carbon, 36, 159-175.*

30. *Dombrovskis, J.K.; Jeong, H.Y.; Fossum, K.; Terasaki, O.; Palmqvist, A.E.C. (2013). Transition Metal Ion-Chelating Ordered Mesoporous Carbons as Noble Metal-Free Fuel Cell Catalysts. Chemistry of Materials, 25, 856-861.*

31. *Thambiliyagodage, C.J.; Hakat, Y.; Bakker, M.G. (2016). One pot synthesis of carbon/Ni nanoparticle monolithic composites by nanocasting and their catalytic activity for 4-Nitrophenol reduction. Current Catalysis, 5, 135-146.*

32. *Smått, J.-H.; Schunk, S.A.; Lindén, M. (2003). Versatile Double-Templating Synthesis Route to Silica Monoliths Exhibiting a Multimodal Hierarchical Porosity. Chemistry of Materials, 15, 2354-2361.*

33. *Taguchi, A.; Smått, J.-H.; Lindén, M. (2003). Carbon Monoliths Possessing a Hierarchical, Fully Interconnected Porosity. Advanced Materials, 15, 1209-1211.*

34. *Grano, A.J.; Sayler, F.M.; Smått, J.-H.; Bakker, M.G. (2014). Hierarchically Porous Monoliths of carbon and metal oxides with ordered mesopores Journal of Porous Materials, 21, 1113-1122.*

35. *Ferrari, A.C.; Robertson, J. (2000). Interpretation of Raman spectra of disordered and amorphous carbon. Physical Review B, 61, 14095-14107.*

36. *Cancado, L.G.; Jorio, A.; Martins Ferreira, E.H.; Stavale, F.; Achete, C.A.; Capaz, R.B.; Moutinho, M.V.O.; Lombardo, A.; Kulmala, T.S.; Ferrari, A.C. (2011). Quantifying Defects in Graphene via Raman Spectroscopy at Different Excitation Energies. Nano Letters, 11, 3190–3196.*

37. *Ferrari, A.C.; Robertson, J. (2001). Resonant Raman spectroscopy of disordered, amorphous, and diamondlike carbon. Physical Review B, 64, 075414-075411-075413.*

38. *Jawhari, T.; Roid, A.; Casado, J. (1995). Raman Spectroscopic Characterization of Some Commercially Available Carbon Black Materials. Carbon, 33, 1561-1565.*

39. *Nistor, L.C.; Van Landuyt, J.; Ralchenko, V.G.; Kononenko, T.V.; Obraztsova, E.D.; Streinitsky, V.E. (1994). Direct Observation of Laser-Induced Crystallization of a-C: H Films. Applied Physics. A, 58, 137-144.*

40. *Ferrari, A.C.; Robertson, J. (2004). Raman spectroscopy of amorphous, nanostructured, diamond-like carbon, and nanodiamond. Philosophical Transactions of the Royal Society, 362, 2477-2512.*

41. *Bulusheva, L.G.; Okotrub, A.V.; Kinloch, I.A.; Asanov, I.P.; Kurenya, A.G.; Kudashov, A.G.; Chen, X.; Song, H. (2008). Effect of nitrogen doping on Raman spectra of multi-walled carbon nanotubes. Physica Status Solidi B, 245, 1971-1974.*

42. *Hellgren, N.; Haasch, R.T.; Schmidt, S.; Hultman, L.; Petrov, I. (2016). Interpretation of X-ray photoelectron spectra of carbon-nitride thin films: New insights from in situ XPS. Carbon, 108, 242-252.*

43. *Wu, M.; Feng, Q.; Sun, X.; Wang, H.; Gielen, G.; Wu, W. (2015). Rice (Oryza sativa L) plantation affects the stability of biochar in paddy soil. Scietific Reports, 5, 10001-10010.*

44. *Bertoti, I.; Mohai, M.; Laszlo, K. (2015). Surface modification of graphene and graphite by nitrogen plasma: Determination of chemical state alterations and assignments by quantitative X-ray photoelectron spectroscopy. Carbon, 84, 185-196.*

45. *Ibrahim, E.M.M.; Khavrus, V.O.; Leonhardt, A.; Hampel, S.; Oswald, S.; Rümmeli, M.H.; Büchner, B. (2010). Synthesis, characterization, and electrical properties of nitrogen-doped single-walled carbon nanotubes with different nitrogen content. Diamond and Relatted Materials, 19, 1199-1206.*

46. *Wang, S.; Wang, J.; Zhao, Q.; Li, D.; Wang, J.-Q.; Cho, M.; Cho, H.; Terasaki, O.; Chen, S.; Wan, Y. (2015). Highly Active Heterogeneous 3 nm Gold Nanoparticles on Mesoporous Carbon as Catalysts for Low-Temperature Selective Oxidation and Reduction in Water. ACS Catalysis, 5, 797-802.*

47. *Jawale, D.V.; Gravel, E.; Geertsen, V.r.; Li, H.; Shah, N.; Kumar, R.; John, J.; Namboothiri, I.N.N.; Doris, E. (2014). Size effect of gold nanoparticles supported on carbon nanotube as catalysts in selected organic reactions. Tetrahedron, 6140-6145.*

48. *Li, X.-H.; Wang, X.; Antonietti, M. (2012). Solvent-Free and Metal-Free Oxidation of Toluene Using O2 and g-C3N4 with Nanopores: Nanostructure Boosts the Catalytic Selectivity. ACS Catalysis, 2, 2082-2086.*

49. *Lu, A.-H.; Smått, J.-H.; Backlund, S.; Lindén, M. (2004). Easy and flexible preparation of nanocasted carbon monoliths exhibiting a multimodal hierarchical porosity. Microporous and Mesoporous Materilas, 72, 59-65.*

50. *Lu, A.-H.; Smått, J.-H.; Lindén, M. (2005). Combined Surface and Volume Templating of Highly Porous Nanocast Carbon Monoliths. Advanced Funcional Materials, 15, 865-871.*

51. *Brunauer, S.; Emmett, P.H.; Teller, E. (1938). Adsorption of Gases in Multimolecular Layers. Journal of American Chemical Society, 60, 309-319.*

52. *Barrett, E.P.; Joyner, L.G.; Halenda, P.P. (1951). The Determination of Pore Volume and Area Distributions in Porous Substances. I. Computations from Nitrogen Isotherms. Journal of American Chemical Society, 73, 373-380.*